INORGANIC CHEMISTRY
FRONTIERS

CHINESE CHEMICAL SOCIETY
ROYAL SOCIETY OF CHEMISTRY

RESEARCH ARTICLE

View Article Online
View Journal | View Issue

Cite this: *Inorg. Chem. Front.*, 2023, **10**, 3367

Stereochemically active lone-pair-driven giant enhancement of birefringence from three-dimensional $CsZn_4Ga_5Se_{12}$ to two-dimensional $CsZnAsSe_3$†

Chao Zhang,‡[a] Mao-Yin Ran,‡[b,c,d] Xin Chen,[a] Sheng-Hua Zhou,[b,c,d] Hua Lin *[b,c] and Yi Liu *[a]

Received 17th March 2023,
Accepted 27th April 2023

DOI: 10.1039/d3qi00504f

rsc.li/frontiers-inorganic

Birefringent crystals are highly desirable for their important applications in optoelectronic fields. However, the rational design of novel birefringent materials with large birefringence (Δ*n*) has always faced great challenges. In this work, a novel quaternary thioarsenate, $CsZnAsSe_3$, has been rationally designed and successfully obtained based on a stereochemically active lone pair (SCALP) induction strategy *via* the facile surfactant–thermal method. In the structure of $CsZnAsSe_3$, isolated $[AsSe_3]$ triangular pyramids and one-dimensional infinite $[Zn–Se]_\infty$ chains are alternately connected with each other to generate a two-dimensional $[ZnAsSe_3]^-$ layer and the charge-balanced Cs^+ cations are occupied between them. The introduction of SCALP cations not only induces structural dimension transformation but also significantly improves optical anisotropy. Remarkably, $CsZnAsSe_3$ exhibits a significantly increased Δ*n* (*ca.* 0.223), which is about 28 times that of the previously reported three-dimensional parent $CsZn_4Ga_5Se_{12}$ (*ca.* 0.008). Moreover, detailed theoretical investigation has aided in the deep understanding of the electronic structure and the source of large Δ*n*. This research offers a useful structural design strategy for discovering new chalcogenides with enhanced Δ*n* in the future.

Introduction

Birefringent crystals have attracted continuously intensive studies owing to their capability of modulating the polarization of light and they are critically important for many optoelectronic fields such as optical communication, polarization information processing and laser polarization technology.[1] To date, commercially leading birefringent crystals have been mainly used in oxides, such as α-BaB_2O_4 (0.2–2.5 μm),[2] $CaCO_3$ (0.35–2.3 μm),[3] YVO_4 (0.4–5 μm),[4] and $LiNbO_3$ (0.42–5.2 μm),[5] and widely used in the spectral interval from UV to near-IR. Unfortunately, the disadvantageous absorption of the M–O bonds limits their further application in mid- and far-IR regions. Therefore, there is a very urgent need to discover novel mid- and far-IR birefringent crystals with large birefringence (Δ*n*).

In terms of the structure–active relationship, Δ*n* is largely dependent on the anisotropic polarization of the crystal structures.[6] Over the last ten years, various structural design strategies have been widely applied to discover excellent birefringent crystals. Among them, stereochemically active lone pair (SCALP) induction is one of the most useful strategies.[7] For example, by reacting HIO_3 with potassium sulfate, $K_2SO_4 \cdot HIO_3$ has been successfully obtained by Ok and co-workers and it displays a 70 times increase in Δ*n* when compared to K_2SO_4 at 589.3 nm.[8] Another classic example, Sn_2PO_4X (X = Cl, Br, and I), was discovered by Pan's group by introducing Sn(II)–O–X groups into phosphates, which displayed enhanced Δ*n* of larger than 0.2 at 1064 nm.[9] Recently, Zou's group found that Sb(III)-based sulfates and phosphates, such as $CsSbSO_4F_2$ and $K_2SbP_2O_7F$, respectively, show dramatically improved Δ*n*.[10] Benefiting from the wide transmission range and rich structural chemistry, metal chalcogenides are considered one of the best candidates for developing new MIR and FIR birefringent crystals.[11] Although some chalcogenide birefringent crystals

---

[a] *Institute for Composites Science Innovation (InCSI), School of Materials Science and Engineering, Zhejiang University, Hangzhou 310027, China. E-mail: liuyimse@zju.edu.cn*
[b] *Fujian Science & Technology Innovation Laboratory for Optoelectronic Information of China, Fuzhou, Fujian 350108, China. E-mail: linhua@fjirsm.ac.cn*
[c] *State Key Laboratory of Structural Chemistry, Fujian Institute of Research on the Structure of Matter, Chinese Academy of Sciences, Fuzhou, Fujian 350002, China*
[d] *University of Chinese Academy of Sciences, Beijing 100049, China*

† Electronic supplementary information (ESI) available: Additional crystallographic data, CIF files, experimental and theory results, together with additional tables and figures. CCDC 2215339. For ESI and crystallographic data in CIF or other electronic format see DOI: https://doi.org/10.1039/d3qi00504f

‡ C. Zhang and M. Y. Ran contributed equally to this work.

have been discovered recently, obtaining novel chalcogenides with large Δ*n* by the SCALP induction strategy based on the known structure is rarely reported.

The well-known quaternary polar I–II_4–III_5–Q_{12} (I = K, Rb, and Cs; II = Mn, Zn, and Cd; III = Ga and In; Q = S, Se, and Te), is a large family of IR nonlinear optical (NLO) candidates featuring three-dimensional (3D) networks and exhibits remarkable second-harmonic-generation effects.[12] Unfortunately, most of them cannot realize effective phase-matching in the IR region owing to their too small Δ*n*. To obtain improved Δ*n*, a series of new chalcogenides, such as $KHg_4Ga_5Se_{12}$,[13] $AM^{II}_3Ga_5S_{11}$ (A = K, Rb, and Cs; M^{II} = Mn and Cd),[14] and $AM^{III}Sn_2Se_6$ (A = Rb and Cs; M^{III} = Ga and In),[15] has been designed and successfully prepared by different structural strategies with the I–II_4–III_5–Q_{12} type compounds as the template in the past ten years. However, the improvement of the Δ*n* of the aforementioned compounds is not very significant, which can be attributed to the fact that all materials retain the 3D diamond-like frameworks with poor anisotropy in the parent structure. It is widely known that the anisotropic polarization of the crystal structure is the key factor for Δ*n*. Therefore, finding ways to obtain a low-dimensional structure with significant anisotropy is the most effective strategy to achieve large Δ*n* values of materials.[16]

Driven by the above-mentioned SCALP induction strategy, a novel quaternary thioarsenate with a two-dimensional (2D) layered structure, namely, $CsZnAsSe_3$ has been successfully obtained by a facile surfactant–thermal method, which exhibits significantly improved Δ*n* (*ca.* 0.223) when compared to the parent $CsZn_4Ga_5Se_{12}$ (*ca.* 0.008). Moreover, we show the detailed investigations of crystal synthesis, structural evolution, optical characterization, and theoretical calculations to aid the understanding of the electronic structure and the source of large Δ*n*.

Experimental section

Synthesis and characterization

The starting reagents $CsOH·H_2O$ (2 N), Zn powder (3 N), 1,2-propanediamine and PEG-400 were purchased from Sinopharm Chemical Reagent Co., Ltd. Se (4 N) and As_2Se_3 (3 N) were purchased from Aladdin Co., Ltd. The aforementioned chemicals were directly used for the reaction without further purification. Compound $CsZnAsSe_3$ was used in the reaction as follows: 1 mmol of $CsOH·H_2O$, 0.4 mmol of Zn, 0.5 mmol of As_2Se_3, 2.5 mmol of Se, 2.0 mL of PEG-400 and 1 mL of 1,2-propanediamine. All reactants were sealed in a 25 mL Teflon-lined stainless autoclave, which was held at 453 K for one week, and then naturally cooled to room temperature. The reaction mixture was washed with distilled water and ethanol, respectively. A large number of yellow block-shaped $CsZnAsSe_3$ crystals (close to 40% yield based on Zn) were discovered and a pure phase could be easily obtained by manually selecting crystals from the mixture. Single-crystal XRD data of $CsZnAsSe_3$ were collected using an Oxford Xcalibur (Atlas Gemini ultra) diffractometer with graphite-monochromated Mo-K_α radiation (λ = 0.71073 Å) at 273 K. Elemental analysis was performed using an EDX-equipped JEOL/JSM-6360A SEM. Powder XRD data were obtained on a Bruker D8 Advance diffractometer with graphite-monochromatized Cu-K_α radiation. Thermogravimetry (TG) analysis was performed under a flowing N_2 atmosphere at 313–1273 K using a NETZSCH STA 449C simultaneous analyzer. The optical band gap was collected on a Hitachi UH4150 UV-vis-NIR spectrometer equipped with an integrating sphere from 200 nm to 2500 nm. The birefringence of the single-crystal $CsZnAsSe_3$ was observed using a ZEISS Axio A1 polarizing microscope. Theoretical results were also carried out based on the DFT method (see the ESI† for the detailed discussion).

Results and discussion

$CsZn_4Ga_5Se_{12}$ belongs to the acentric *R*3 (no. 146) trigonal space group and possesses the following crystallographically unique positions in its asymmetric unit: 1 Cs, 3 M (M = Zn/Ga) and 4 Se atoms. Each M is bonded with 4 Se atoms to give rise to an $[MSe_4]$ tetrahedron which has 4 normal M–Se bonds with 2.379(3)–2.482(2) Å bond lengths. The Cs atom coordinates with 12 Se atoms to generate a cuboctahedron, showing the Cs–Se bond lengths of 3.769(2)–3.843(3) Å (Fig. S1†). Three $[M(2)Se_4]$ tetrahedra are arranged in a six-membered ring and alternately interconnected with other $[M(1)Se_4]$ and $[M(3)Se_4]$ tetrahedra, creating an $[M_9Se_{24}]$ functional primitive (Fig. 1a). These functional primitives are interconnected *via* Se-sharing to form 2D $[Zn_4Ga_5Se_{12}]^-$ layers (Fig. 1b) that are further interlinked *via* M–Se–M bonds to construct a 3D diamond-like framework, in which charge-balanced Cs^+ cations are filled between the 2D layers (Fig. 1c). Regrettably, such a dense 3D framework structure with poor anisotropy results in an extremely low Δ*n* of $CsZn_4Ga_5Se_{12}$.

$CsZnAsSe_3$ crystallizes in the monoclinic system with the centrosymmetric space group of $P2_1/c$ (no. 14) (Table 1). Each asymmetric unit contains 1 independent Cs site (Wyckoff position: 4*e*), 1 Zn site (4*e*), 1 As site (4*e*), and 3 Se sites (4*e*) (Table 2). The coordination modes of Zn and As atoms are given in Fig. 1d. The selected bond distances and angles are shown in Table S1.† The bond lengths of Zn–Se in $[ZnSe_4]$ are in the range of 2.444–2.532 Å, while the As–Se bond lengths in $[AsSe_3]$ are between 2.360 and 2.420 Å (Fig. 1d). Two $[ZnSe_4]$ tetrahedra are interconnected with each other through Se-sharing to build $[Zn_2Se_7]^{10-}$ dimers that are further interlinked *via* Zn–Se–Zn bonds to construct a wave one-dimensional (1D) infinite $[Zn–Se]_\infty$ chain extending along the *b* axis. These 1D $[Zn–Se]_\infty$ chains further form a 2D $[ZnAsSe_3]$ layer with discrete $[AsSe_3]$ triangular pyramids (Fig. 1e), with Cs^+ acting as a charge-balanced cation located between these layers (Fig. 1f). Compared with the Cs atom that centers the Se_{12} cuboctahedron in the $CsZn_4Ga_5Se_{12}$, the Cs atoms are coordinated by 8 Se atoms to generate a highly twisted $CsSe_8$ bicapped trigonal prism in $CsZnAsSe_3$ (Fig. S2 in the ESI†). Similar examples are

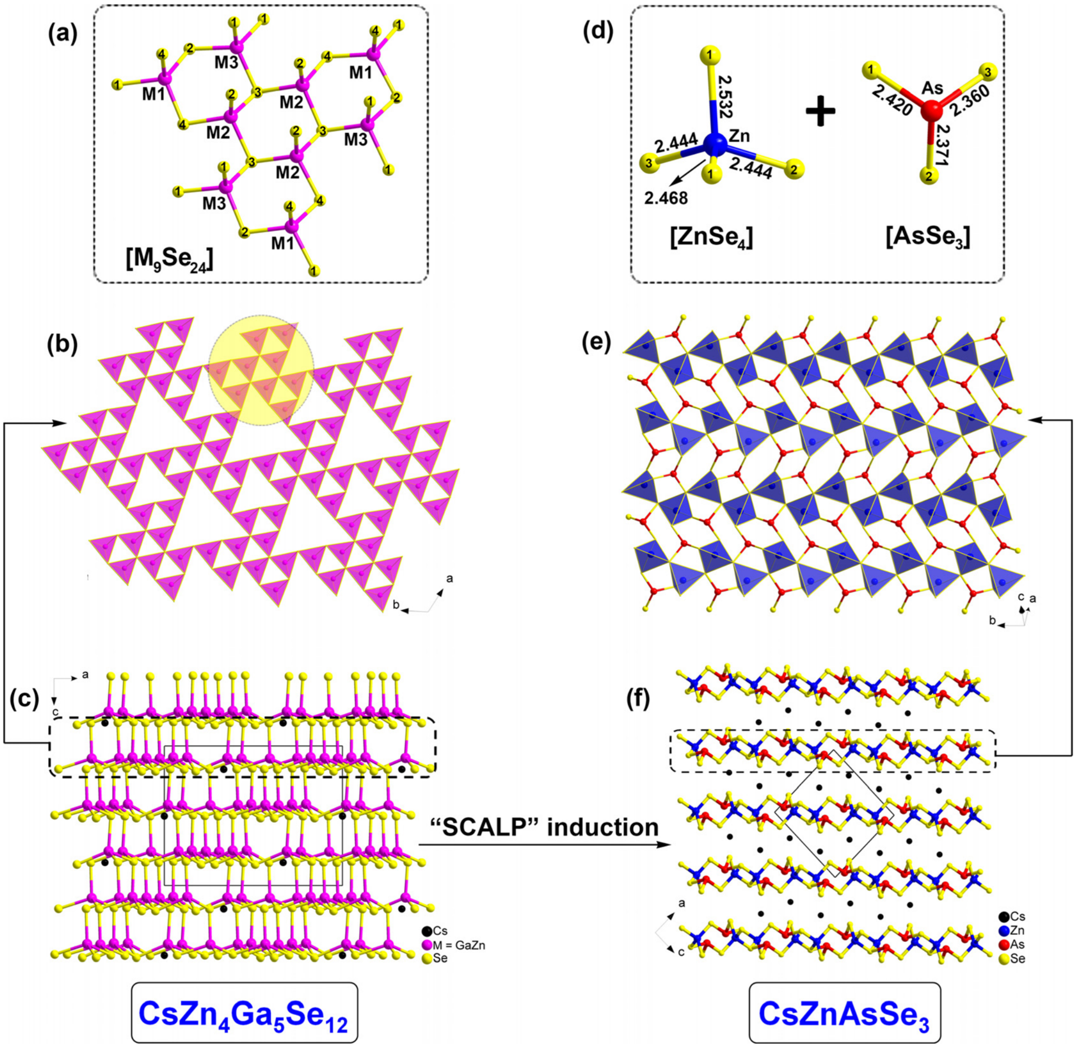

Fig. 1 Structural evolution from 3D $CsZn_4Ga_5Se_{12}$ to 2D $CsZnAsSe_3$: (a and d) coordination environment of $[M_9Se_{24}]$ (M = Zn/Ga), $[ZnSe_4]$ and $[AsSe_3]$ FBBs with the atom numbers and bond distance marked; (b and e) projection of 2D $[Zn_4Ga_5Se_{12}]^-$ and 2D $[ZnAsSe_3]^-$ layers along the *ab*- and *ac*-planes, respectively; (c and f) the ball-and-stick models of 3D $CsZn_4Ga_5Se_{12}$ and 2D $CsZnAsSe_3$ with the unit cell outlined.

also found in some other Cs-based chalcogenides.[17] It is interesting to note that the selenide of $CsZnAsSe_3$ is the first quaternary phase discovered within the A–Zn–As–Q (A = alkali metals; Q = chalcogen) systems.

Structural evolution from 3D $CsZn_4Ga_5Se_{12}$ to 2D $CsZnAsSe_3$ based on the SCALP induction strategy is illustrated in Fig. 1. $CsZnAsSe_3$ might be considered the two-step substitution compound from $CsZn_4Ga_5Se_{12}$. First, the tetrahedral $[GaSe_4]$ basic building units are replaced by $[AsSe_3]$ triangular pyramids. Second, the charge shortage caused by the reduction of the coordination number is supplemented by charge-balanced Cs^+ cations. Similar structural evolution processes can be found in some other chalcogenide systems.[18] From the point of chemical design, the As atom was chosen to change the crystal structure owing to the following considerations: (i) As and Ga belong to the same period and the ionic radius is close to ($r(As^{3+})$ = 0.58 Å *vs.* $r(Ga^{3+})$ = 0.62 Å). Theoretically, free substitution can be realized between them according to the Goldschmidt rule.[19] (ii) The introduction of SCALP groups is conducive to symmetry breaking and thereby obtaining a low-dimensional structure. (iii) The highly polarizable As–Se bond is beneficial for the improvement of Δn.[20]

Single crystals of $CsZnAsSe_3$ were prepared by the facile surfactant–thermal method[21] and yellow block-shaped crystals were chosen for characterization. The elemental distribution of Cs : Zn : As : Se was determined to be 1 : 1.0(1) : 1.2(2) : 2.9(1) by EDX mapping (Fig. S3, ESI†), which is close to the result of single-crystal XRD analysis. In addition, the phase of $CsZnAsSe_3$ was verified by powder XRD measurements, as shown in Fig. 2a. The results indicate that the experimental patterns match well with the simulated ones derived from the CIF data. The result of the UV-Vis-NIR diffuse reflectance spectrum shows that the experimental energy gap (E_g) is about 2.25 eV for $CsZnAsSe_3$ (Fig. 2b), which is wider than those of other

Table 1 Crystallographic information and refinement results for $CsZnAsSe_3$

Empirical formula	$CsZnAsSe_3$
CCDC number	2215339
Formula weight	510.08
Temperature (K)	293(2)
Crystal system	Monoclinic
Space group	$P2_1/c$ (no. 14)
a (Å)	10.2443(4)
b (Å)	6.6430(3)
c (Å)	10.6276(5)
α (°)	90
β (°)	93.871(4)
γ (°)	90
V (Å^3)	721.59(5)
Z	4
D_c (g cm^{-3})	4.695
μ (mm^{-1})	44.141
GOOF on F^2	1.102
R_1, wR_2 ($I > 2\sigma(I)$)[a]	0.0457, 0.1219
R_1, wR_2 (all data)	0.0467, 0.1226
Largest diff. peak and hole (e Å^{-3})	3.312, −2.944

[a] $R_1 = \sum||F_o| - |F_c||/\sum|F_o|$, $wR_2 = [\sum w(F_o^2 - F_c^2)^2/\sum w(F_o^2)^2]^{1/2}$.

Table 2 The atomic coordinates and equivalent isotropic displacement parameters for $CsZnAsSe_3$

Atom	Wyckff.	x	y	z	U_{eq}/Å^2
Cs	4e	0.07666(4)	0.80032(7)	0.67533(4)	0.0064(2)
Zn	4e	0.33503(2)	0.19131(2)	0.34814(2)	0.0024(3)
As	4e	0.38109(8)	0.66019(2)	0.46021(8)	0.0024(2)
Se1	4e	0.21283(8)	0.87236(2)	0.35947(7)	0.0027(2)
Se2	4e	0.24498(7)	0.38994(2)	0.51540(7)	0.0038(2)
Se3	4e	0.42689(8)	0.82296(2)	0.65564(8)	0.0042(2)

U_{eq} is defined as one-third of the trace of the orthogonalized U_{ij} tensor.

reported quaternary alkali metal-based thioarsenates, including $K_7As_3(P_2Se_6)_4$ (E_g = 2.0 eV),[22] $Cs_3CuAs_4Se_8$ (E_g = 1.83 eV),[23] $K_2Sm_2As_2Se_9$ (E_g = 1.70 eV),[24] $K_3BiAs_6Se_{12}$ (E_g = 1.65 eV),[25] and $RbAg_2As_3Se_6$ (E_g = 1.44 eV).[26] Besides, $CsZnAsSe_3$ exhibits desirable thermal stability (up to 900 K) under N_2 conditions according to the TG curve, as shown in Fig. 2c. Additionally, the optical transmittance spectra of $CsZnAsSe_3$ are depicted in Fig. S4,† indicating that no bond absorption occurs in a broad spectral range from 0.44 to 25 μm, which covers two important atmospheric transparent windows (3–5 and 8–14 μm). Such a result suggests that $CsZnAsSe_3$ may be suitable for applications in the mid- and far-IR regions.

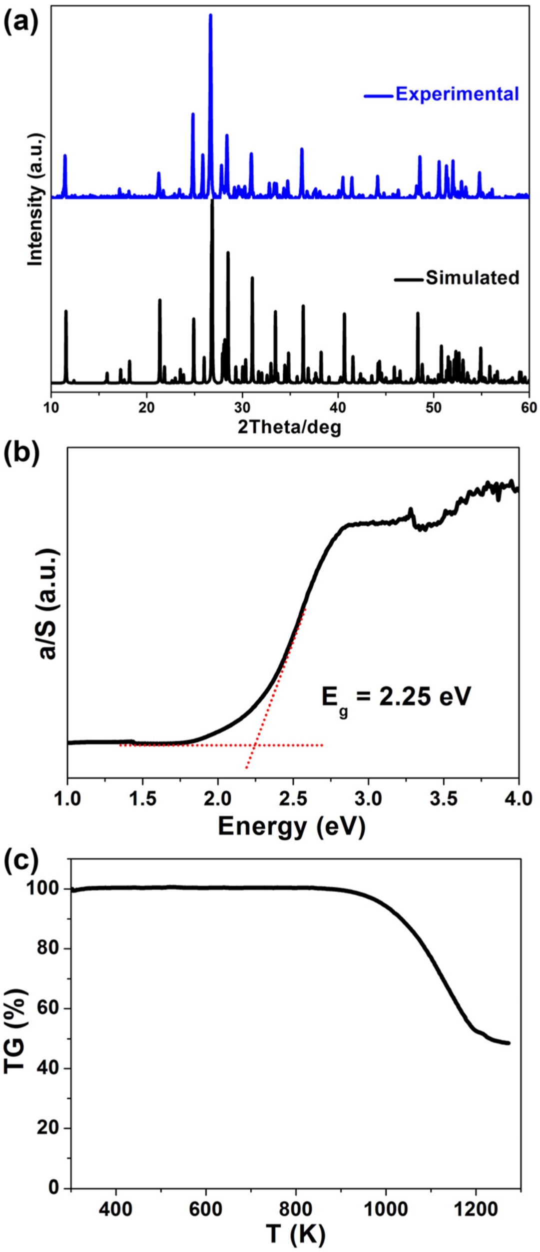

Fig. 2 Experimental characterization of $CsZnAsSe_3$: (a) powder XRD patterns, (b) the reflectance spectrum transformed using the Kubelka–Munk function and (c) TG curve.

Furthermore, the Δn of $CsZn_4Ga_5Se_{12}$ and $CsZnAsSe_3$ was observed using a ZEISS Axio A1 cross-polarizing microscope. The observed interference colours of $CsZn_4Ga_5Se_{12}$ and $CsZnAsSe_3$ at 546 nm under cross-polarized light are shown in Fig. 3. In terms of the Michel–Levy chart, their retardations (R values) and crystal thicknesses (T values) were measured as 117 nm and 13.8 μm for $CsZn_4Ga_5Se_{12}$ and 1381 nm and 6.2 μm for $CsZnAsSe_3$, respectively. Therefore, their Δn values in the visible range were calculated as 0.008 for $CsZn_4Ga_5Se_{12}$ and 0.223 for $CsZnAsSe_3$ based on the formula of $\Delta n = R/T$.[27] It is worth recalling that the experimental Δn shows about a 28 times increase for 2D $CsZnAsSe_3$ compared to that of 3D $CsZn_4Ga_5Se_{12}$. Notably, the Δn of $CsZnAsSe_3$ is close to or higher than those of most commercial birefringent materials, such as YVO_4 (0.23 at 630 nm),[4] α-BaB_2O_4 (0.12 at 544 nm),[2] and $LiNbO_3$ (0.08 at 632 nm),[5] and also larger than those of many recently reported chalcogenides, such as $LiBaSbS_3$ (0.05 at 532 nm),[28] α-$CsBa_2SnSe_4Cl$ (0.06 at 532 nm),[29] $K_2Na_2Sn_3S_8$ (0.07 at 546 nm),[30] $Cs_2ZnSn_3S_8$ (0.12 at 546 nm),[31] β-$CsBa_2SnSe_4Cl$ (0.14 at 532 nm)[29] and $Rb_3NaSn_3Se_8$ (0.20 at

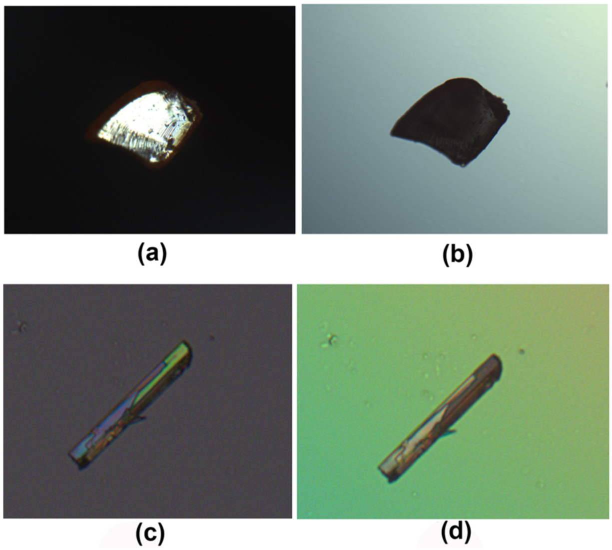

Fig. 3 (a and b) $CsZn_4Ga_5Se_{12}$ and (c and d) $CsZnAsSe_3$ crystals for Δn determination and the interference colors observed before and after complete extinction.

546 nm),[30] suggesting that it has potential as an IR birefringent candidate. This result suggests that the SCALP induction strategy is very effective for improving optical anisotropy and enhancing Δn in chalcogenide systems.

Furthermore, the detailed energy band structure and partial density of states (PDOS) have aided in a better understanding of the electronic structure and the source of large Δn. It is evident from Fig. 4a that the valence band maximum (VBM) and the conduction band minimum (CBM) occupy the same G points, suggesting that $CsZnAsSe_3$ is a direct band-gap semiconductor. The calculated E_g of 1.97 eV is slightly less than the corresponding experimental value of 2.25 eV, which can be attributed to the well-known discontinuity of exchange correction energy in the GGA.[32] The PDOS analysis of $CsZnAsSe_3$ was performed as shown in Fig. 4b. As can be seen, the top of the VBs mainly consists of Se-4p states, while the bottom of CBs mainly consists of Cs-6d, Zn-4s/3p/3d, and As-4s/4p orbital states. The high density and overlap of the Zn-4s/3p/3d, As-4s/4p, and Se-4p orbitals near the Fermi level (E_F is fixed to 0 eV, *i.e.*, $E_{VBM} = 0$) reveal that $[AsSe_3]$ triangular pyramids and $[ZnSe_4]$ tetrahedra mainly determine the optical E_g of the structure.

On the basis of the electronic structure, we also calculated the Δn values of $CsZn_4Ga_5Se_{12}$ and $CsZnAsSe_3$, respectively. The calculated result is shown in Fig. 5a. It can be

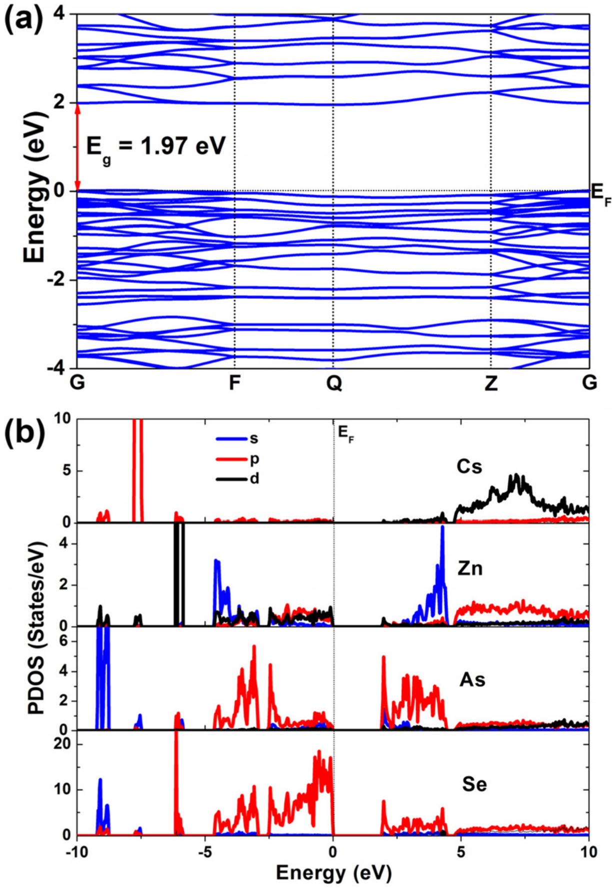

Fig. 4 Theoretical calculations of $CsZnAsSe_3$: (a) calculated band structure and (b) PDOS.

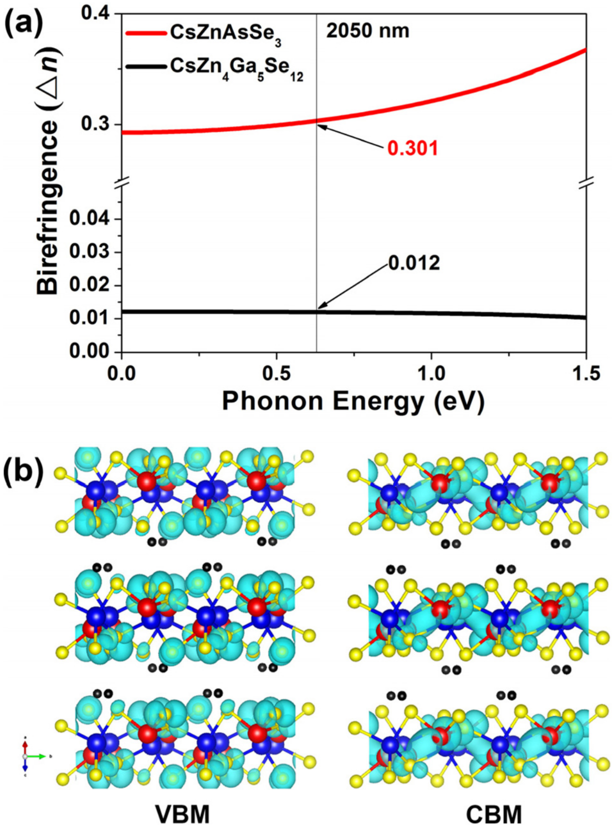

Fig. 5 (a) Calculated birefringence of $CsZnAsSe_3$. (b) Projection of the partial charge density maps in the VBM and CBM parts.

seen that their Δ*n* values at 2050 nm are 0.012 and 0.301 for $CsZn_4Ga_5Se_{12}$ and $CsZnAsSe_3$, respectively. The increase of Δ*n* from $CsZn_4Ga_5Se_{12}$ to $CsZnAsSe_3$ is very consistent with the structural analysis and experimental results. Moreover, partial charge density maps in the VBM and CBM parts to visualize the distribution of the bonding and SCALP electrons are given in Fig. 5b. It confirms the strong lone electron density clouds around the As^{3+} cations and the optical anisotropy is closely related to the $[AsSe_3]$ unit arrangement modes.

Conclusions

In summary, a novel birefringent crystal containing a 2D unique layered structure, $CsZnAsSe_3$, has been successfully designed by the SCALP induction strategy and synthesized by the surfactant–thermal reaction. In particular, the birefringence of $CsZnAsSe_3$ is about 28 times higher than that of previously reported $CsZn_4Ga_5Se_{12}$ with a dense 3D framework structure, which can be attributed to the successful introduction of SCALP $[AsSe_3]$ triangular pyramids. Our study not only offers a deep understanding of the role of the SCALP effect in the birefringence property of $CsZnAsSe_3$ but also suggests that the $CsZnAsSe_3$ crystal may be used for polarization-dependent optical applications.

Author contributions

C. Zhang designed and carried out the experiments and finished the manuscript. M. Y. Ran performed the characterization of optical properties. X. Chen prepared the samples. S. H. Zhou carried out the theoretical calculations. H. Lin and Y. Liu analyzed the results and edited the manuscript. All the authors have approved the final version of the manuscript. C. Zhang and M. Y. Ran contributed equally to this work.

Conflicts of interest

There are no conflicts to declare.

Acknowledgements

This research was supported by the National Natural Science Foundation of China (52171277 and 22175175), the Fujian Science & Technology Innovation Laboratory for Optoelectronic Information of China (2021ZR118), the Natural Science Foundation of Fujian Province (2022L3092) and the Shanxi-Zheda Institute of Advanced Materials and Chemical Engineering (2022SZ-TD006).

References

1 (*a*) Z. Xie, L. Sun, G. Han and Z. Gu, Optical Switching of a Birefringent Photonic Crystal, *Adv. Mater.*, 2008, **20**, 3601–3604; (*b*) S. Niu, J. Graham, H. Zhao, Y. Zhou, O. Thomas, H. Huaixun, S. Jad, M. Krishnamurthy, U. Brittany and J. Wu, Giant optical anisotropy in a quasi-one-dimensional crystal, *Nat. Photonics*, 2018, **12**, 392–396; (*c*) X. Chen, W. G. Lu, J. Tang, Y. Zhang, Y. Wang, G. D. Scholes and H. Zhong, Solution-processed inorganic perovskite crystals as achromatic quarter-wave plates, *Nat. Photonics*, 2021, **15**, 813–816; (*d*) Y. Zhou, X. Zhang, M. Hong, J. Luo and S. Zhao, Achieving effective balance between bandgap and birefringence by confining π-conjugation in an optically anisotropic crystal, *Sci. Bull.*, 2022, **67**, 2276–2279; (*e*) N. Berti, S. Coen, M. Erkintalo and J. Fatome, Extreme waveform compression with a nonlinear temporal focusing mirror, *Nat. Photonics*, 2022, **16**, 822–827.

2 G. Zhou, J. Xu, X. Chen, H. Zhong and F. Gan, Growth and spectrum of a novel birefringent α-BaB_2O_4 crystal, *J. Cryst. Growth*, 1998, **191**, 517–519.

3 G. Ghosh, Dispersion-equation coefficients for the refractive index and birefringence of calcite and quartz crystals, *Opt. Commun.*, 1999, **163**, 95–102.

4 H. Luo, T. Tkaczyk, E. Dereniak and K. Oka, High birefringence of the yttrium vanadate crystal in the middle wavelength infrared, *Opt. Lett.*, 2006, **31**, 616–618.

5 D. E. Zelmon, D. L. Small and D. Jundt, Infrared corrected Sellmeier coefficients for congruently grown lithium niobate and 5 mol% magnesium oxide-doped lithium niobate, *J. Opt. Soc. Am. B*, 1997, **14**, 3319–3322.

6 (*a*) A. Tudi, S. Han, Z. Yang and S. Pan, Potential optical functional crystals with large birefringence: Recent advances and future prospects, *Coord. Chem. Rev.*, 2022, **459**, 214380; (*b*) Q. Shi, L. Dong and Y. Wang, Evaluating refractive index and birefringence of nonlinear optical crystals: Classical methods and new developments, *Chin. J. Struct. Chem.*, 2023, **42**, 100017; (*c*) J. Zhang, C. Wu, H. Shi, C. Xie, Z. Yang and S. Pan, An interlinked prediction-experiment paradigm discovering deep-ultraviolet fluorooxoborates with desired optical nonlinearity and birefringence, *Matter*, 2023, DOI: **10.1016/j.matt.2023.02.005**; (*d*) F. Zhang, X. Chen, M. Zhang, W. Jin, S. Han, Z. Yang and S. Pan, An excellent deep-ultraviolet birefringent material based on $[BO_2]_\infty$ infinite chains, *Light: Sci. Appl.*, 2022, **11**, 252.

7 (*a*) S. Han, A. Tudi, W. Zhang, X. Hou, Z. Yang and S. Pan, Recent Development of Sn(II), Sb(III)-based Birefringent Material: Crystal Chemistry and Investigation of Birefringence, *Angew. Chem., Int. Ed.*, 2023, DOI: **10.1002/anie.202302025**; (*b*) H. Lin, Y. Y. Li, M. Y. Li, Z. J. Ma, L. M. Wu, X. T. Wu and Q. L. Zhu, Centric-to-acentric structure transformation induced by a stereochemically active lone pair: a new insight for design of IR nonlinear optical materials, *J. Mater. Chem. C*, 2019, **7**, 4638–4643; (*c*) Y. Liu, X. Liu, S. Liu, Q. Ding, Y. Li, L. Li, S. Zhao, Z. Lin, J. Luo

and M. Hong, An Unprecedented Antimony(III) Borate with Strong Linear and Nonlinear Optical Responses, *Angew. Chem., Int. Ed.*, 2020, 7793–7796.

8 Z. Bai and K. M. Ok, Dramatically improved optical anisotropy by realizing stereochemically active lone pairs in a sulfate system, $K_2SO_4 \cdot HIO_3$, *Inorg. Chem. Front.*, 2023, **10**, 1919–1925.

9 J. Guo, A. Tudi, S. Han, Z. Yang and S. Pan, Sn_2PO_4I: an excellent birefringent material with giant optical anisotropy in non π-conjugated phosphate, *Angew. Chem., Int. Ed.*, 2021, **60**, 24901–24904.

10 (*a*) X. Dong, L. Huang, C. Hu, H. Zeng, Z. Lin, X. Wang, K. M. Ok and G. Zou, $CsSbF_2SO_4$: an excellent ultraviolet nonlinear optical sulfate with a $KTiOPO_4$ (KTP)-type structure, *Angew. Chem., Int. Ed.*, 2019, **58**, 6528–6534; (*b*) Y. Deng, L. Huang, X. Dong, L. Wang, K. M. Ok, H. Zeng, Z. Lin and G. Zou, $K_2Sb(P_2O_7)F$: Cairo pentagonal layer with bifunctional genes reveal optical performance, *Angew. Chem., Int. Ed.*, 2020, **59**, 21151–21156.

11 (*a*) H. Lin, W. B. Wei, H. Chen, X. T. Wu and Q. L. Zhu, Rational design of infrared nonlinear optical chalcogenides by chemical substitution, *Coord. Chem. Rev.*, 2020, **406**, 213150; (*b*) H. Chen, W. B. Wei, H. Lin and X. T. Wu, Transition-metal-based chalcogenides: A rich source of infrared nonlinear optical materials, *Coord. Chem. Rev.*, 2021, **448**, 214154; (*c*) H. Chen, M. Y. Ran, W. B. Wei, X. T. Wu, H. Lin and Q. L. Zhu, A comprehensive review on metal chalcogenides with three-dimensional frameworks for infrared nonlinear optical applications, *Coord. Chem. Rev.*, 2022, **470**, 214706; (*d*) M. Y. Ran, A. Y. Wang, W. B. Wei, X. T. Wu, H. Lin and Q. L. Zhu, Recent progress in the design of IR nonlinear optical materials by partial chemical substitution: structural evolution and performance optimization, *Coord. Chem. Rev.*, 2023, **481**, 215059.

12 (*a*) H. Lin, L. J. Zhou and L. Chen, Sulfides with Strong Nonlinear Optical Activity and Thermochromism: $ACd_4Ga_5S_{12}$ (A = K, Rb, Cs), *Chem. Mater.*, 2012, **24**, 3406–3414; (*b*) H. Lin, L. Chen, L. J. Zhou and L. M. Wu, Functionalization Based on the Substitutional Flexibility: Strong Middle IR Nonlinear Optical Selenides $AXII_4XIII_5Se_{12}$, *J. Am. Chem. Soc.*, 2013, **135**, 12914–12921; (*c*) H. Lin, Y. Liu, L. J. Zhou, H. J. Zhao and L. Chen, Strong Infrared NLO Tellurides with Multifunction: $CsXII_4In_5Te_{12}$ (XII = Mn, Zn, Cd), *Inorg. Chem.*, 2016, **55**, 4470–4475; (*d*) H. Lin, H. Chen, Y. J. Zheng, J. S. Yu and L. M. Wu, $AXII_4XIII_5Te_{12}$ (A = Rb, Cs; XII = Mn, Zn, Cd; XIII = Ga, In): quaternary semiconducting tellurides with very low thermal conductivities, *Dalton Trans.*, 2016, **45**, 17606–17609; (*e*) H. Lin, H. Chen, Y. J. Zheng, J. S. Yu, X. T. Wu and L. M. Wu, Coexistence of Strong Second Harmonic Generation Response and Wide Band Gap in $AZn_4Ga_5S_{12}$ (A = K, Rb, Cs) with 3D Diamond-like Frameworks, *Chem. – Eur. J.*, 2017, **23**, 10407–10412; (*f*) H. Lin, Y. J. Zheng, X. N. Hu, H. Chen, J. S. Yu and L. M. Wu, Non-centrosymmetric Selenides $AZn_4In_5Se_{12}$ (A = Rb, Cs): Synthesis, Characterization and Nonlinear Optical Properties, *Chem. – Asian J.*, 2017, **12**, 453–458; (*g*) M. M. Chen, S. H. Zhou, W. B. Wei, X. T. Wu, H. Lin and Q. L. Zhu, $AZn_4Ga_5Se_{12}$ (A = K, Rb, or Cs): Infrared Nonlinear Optical Materials with Simultaneous Large Second Harmonic Generation Responses and High Laser-Induced Damage Thresholds, *Inorg. Chem.*, 2021, **60**, 10038–10046; (*h*) Y. Wang, R. Wang, X. Che, F. Liang, M. Luo, Y. Tang, Y. Cao and F. Huang, Infrared nonlinear optical sulfide $CsCd_4In_5S_{12}$ exhibiting large second harmonic generation response, *J. Mater. Chem. C*, 2022, **10**, 5183–5189.

13 M. Zhou, Y. Yang, Y. Guo, Z. Lin, J. Yao, Y. Wu and C. Chen, Hg-Based Infrared Nonlinear Optical Material $KHg_4Ga_5Se_{12}$ Exhibits Good Phase-Matchability and Exceptional Second Harmonic Generation Response, *Chem. Mater.*, 2017, **29**, 7993–8002.

14 M. M. Chen, S. H. Zhou, W. B. Wei, X. T. Wu, H. Lin and Q. L. Zhu, Phase Matchability Transformation in the Infrared Nonlinear Optical Materials with Diamond-Like Frameworks, *Adv. Opt. Mater.*, 2022, **10**, 2102123.

15 (*a*) H. Lin, L. Chen, J. S. Yu, H. Chen and L. M. Wu, Infrared SHG Materials CsM_3Se_6 (M = Ga/Sn, In/Sn): Phase Matchability Controlled by Dipole Moment of the Asymmetric Building Unit, *Chem. Mater.*, 2017, **29**, 499–503; (*b*) H. Lin, H. Chen, Y. J. Zheng, J. S. Yu, X. T. Wu and L. M. Wu, Two excellent phase-matchable infrared nonlinear-optical materials based on the 3D diamond-like frameworks: $RbGaSn_2Se_6$ and $RbInSn_2Se_6$, *Dalton Trans.*, 2017, **46**, 7714–7721.

16 (*a*) M. Y. Li, Y. X. Zhang, H. Lin, Z. J. Ma, X. T. Wu and Q. L. Zhu, Combined experimental and theoretical investigations of Ba_3GaS_4I: interesting structure transformation originated from the halogen substitution, *Dalton Trans.*, 2019, **48**, 17588–17593; (*b*) M.-Y. Ran, Z. Ma, X.-T. Wu, H. Lin and Q.-L. Zhu, $Ba_2Ge_2Te_5$: a ternary NLO-active telluride with unusual one-dimensional helical chains and giant second-harmonic-generation tensors, *Inorg. Chem. Front.*, 2021, **8**, 4838–4845; (*c*) C. Liu, S. H. Zhou, C. Zhang, Y. Y. Shen, X. Y. Liu, H. Lin and Y. Liu, $CsCu_3SbS_4$: rational design of a two-dimensional layered material with giant birefringence derived from Cu_3SbS_4, *Inorg. Chem. Front.*, 2022, **9**, 478–484; (*d*) M. Zhou, C. Li, X. Li, J. Yao and Y. Wu, $K_2Sn_2ZnSe_6$, $Na_2Ge_2ZnSe_6$, and $Na_2In_2GeSe_6$: A New Series of Quaternary Selenides with Intriguing Structural Diversity and Nonlinear Optical Properties, *Dalton Trans.*, 2016, **45**, 7627–7633.

17 (*a*) M. Y. Li, X. Y. Xie, X. T. Wu, X. F. Li and H. Lin, Quaternary Selenophosphate $Cs_2ZnP_2Se_6$ Featuring Unique One-dimensional Chains and Exhibiting Remarkable Photo-electrochemical Response, *Chin. J. Struct. Chem.*, 2021, **40**, 246–255; (*b*) H. Chen, P.-F. Liu, H. Lin and X.-T. Wu, Ultralow thermal conductivity in the quaternary semiconducting chalcogenide $Cs_4[Ho_{26}Cd_7Se_{48}]$ with an unprecedented closed cavity architecture, *Inorg. Chem. Front.*, 2021, **8**, 1049–1055; (*c*) H. Chen, P.-F. Liu, H. Lin and X.-T. Wu, new type of novel salt-inclusion chalco-

genides with ultralow thermal conductivity, *Chem. Commun.*, 2020, **56**, 15149–15152.

18 (*a*) Y. Dou, Y. Chen, Z. Li, A. K. Iyer, B. Kang, W. Yin, J. Yao and A. Mar, $SrCdGeS_4$ and $SrCdGeSe_4$: Promising Infrared Nonlinear Optical Materials with Congruent-Melting Behaviour, *Cryst. Growth Des.*, 2019, **19**, 1206–1214; (*b*) F. You, F. Liang, Q. Huang, Z. Hu, Y. Wu and Z. Lin, $Pb_2GaF_2(SeO_3)_2Cl$: Band Engineering Strategy by Aliovalent Substitution for Enlarging Bandgap while Keeping Strong Second Harmonic Generation Response, *J. Am. Chem. Soc.*, 2019, **141**, 748–752; (*c*) J. Tang, F. Liang, C. Tang, W. Xing, J. Wu, W. Yin, B. Kang and J. Deng, $SrAgAsS_4$: A Noncentrosymmetric Sulfide with Good Infrared Nonlinear Optical Performance Induced by Aliovalent Substitution from Centrosymmetric $SrGa_2S_4$, *Inorg. Chem.*, 2022, **61**, 9205–9212.

19 V. M. Goldschmidt, The principles of distribution of chemical elements in minerals and rocks, *J. Chem. Soc.*, 1937, 655–673.

20 M.-M. Chen, Z. Ma, B.-X. Li, W.-B. Wei, X.-T. Wu, H. Lin and Q.-L. Zhu, $M_2As_2Q_5$ (M = Ba, Pb; Q = S, Se): A source of infrared nonlinear optical materials with excellent overall performance activated by multiple discrete arsenate anions, *J. Mater. Chem. C*, 2021, **9**, 1156–1163.

21 (*a*) W.-W. Xiong, E. U. Athresh, Y. T. Ng, J. Ding, T. Wu and Q. C. Zhang, *J. Am. Chem. Soc.*, 2013, **135**, 1256–1259; (*b*) W. W. Xiong and Q. C. Zhang, *Angew. Chem., Int. Ed.*, 2015, **54**, 11616–11623; (*c*) C. Liu, Y. Xiao, H. Wang, W. X. Chai, X. F. Liu, D. M. Yan, H. Lin and Y. Liu, One-Dimensional Chains in Pentanary Chalcogenides $A_2Ba_3Cu_2Sb_2S_{10}$ (A = K, Rb, Cs) Displaying a Photocurrent Response, *Inorg. Chem.*, 2020, **59**, 1577–1581; (*d*) D. M. Yan, Y. Xiao, C. Liu, P. P. Hou, W. X. Chai, H. Hosono, H. Lin and Y. Liu, Two new members in the quaternary Cs-Ag-As-S family with different arrangements of Ag–S and As–S asymmetric building units: syntheses, structures, and theoretical studies, *Dalton Trans.*, 2020, **49**, 9743–9750; (*e*) Y. Xiao, S. H. Zhou, R. Yu, Y. Y. Shen, Z. J. Ma, H. Lin and Y. Liu, *Inorg. Chem.*, 2021, **60**, 9263–9267; (*f*) Y. Xiao, M. M. Chen, Y. Y. Shen, P. F. Liu, H. Lin and Y. Liu, *Inorg. Chem. Front.*, 2021, **8**, 2835–2843; (*g*) C. Zhang, S. H. Zhou, Y. Xiao, H. Lin and Y. Liu, Interesting dimensional transition through changing cations as the trigger in multinary thioarsenates displaying variable photocurrent response and optical anisotropy, *Inorg. Chem. Front.*, 2022, **9**, 5820–5827.

22 C. D. Morris and M. G. Kanatzidis, Arsenic-containing chalcophosphate molecular anions, *Inorg. Chem.*, 2010, **49**, 9040–9054.

23 C. Liu, H. D. Yang, P. P. Hou, Y. Xiao, Y. Liu and H. Lin, $Cs_3CuAs_4Q_8$ (Q = S, Se): unique two-dimensional layered inorganic thioarsenates with the lowest Cu-to-As ratio and remarkable photocurrent responses, *Dalton Trans.*, 2022, **51**, 904–909.

24 Y. D. Wu and W. Bensch, $K_2Ln_2As_2Se_9$ (Ln = Sm, Gd): The first quaternary rare-earth selenoarsenate compounds with a 3D framework containing chairlike As_2Se_4 units, *Inorg. Chem.*, 2009, **48**, 2729–2731.

25 Y. D. Wu and W. Bensch, $K_3BiAs_6Se_{12}$: a two-dimensional bismuth selenoarsenate containing crown-shaped anions $(As_3Se_6)_3{}^-$, *J. Alloys Compd.*, 2011, **509**, 4452–4456.

26 M. Wachhold and M. G. Kanatzidis, Condensation of pyramidal $(AsSe_3)_3{}^-$ anions for the construction of polymeric networks: solventothermal synthesis of $K_3AgAs_2Se_5·0.25$ (MeOH), $K_2AgAs_3Se_6$ and $Rb_2AgAs_3Se_6$, *Inorg. Chem.*, 1999, **38**, 3863–3870.

27 (*a*) S. Liu, X. M. Liu, S. G. Zhao, Y. C. Liu, L. N. Li, Q. R. Ding, Y. Q. Li, Z. S. Lin, J. H. Luo and M. C. Hong, An Exceptional Peroxide Birefringent Material Resulting from d–π Interactions, *Angew. Chem., Int. Ed.*, 2020, **59**, 9414–9417; (*b*) Y. X. Chen, Z. X. Chen, Y. Zhou, Y. Q. Li, Y. C. Liu, Q. R. Ding, X. Chen, S. G. Zhao and J. H. Luo, An Antimony (III) Fluoride Oxalate With Large Birefringence, *Chem. – Eur. J.*, 2021, **27**, 4557–4560; (*c*) M.-Y. Ran, S.-H. Zhou, W.-B. Wei, B.-X. Li, X.-T. Wu, H. Lin and Q.-L. Zhu, Rational Design of a Rare-Earth Oxychalcogenide $Nd_3[Ga_3O_3S_3][Ge_2O_7]$ with Superior Infrared Nonlinear Optical Performance, *Small*, 2023, **19**, 2300248.

28 A. Abudurusuli, K. Wu, A. Tudi, Z. Yang and S. Pan, $ABaSbQ_3$ (A = Li, Na; Q = S, Se): Diverse Arrangement Modes of Isolated SbQ_3 Ligands Regulating the Magnitudes of Birefringences, *Chem. Commun.*, 2019, **55**, 5143–5146.

29 Y. Chu, K. Wu, X. Su, J. Han, Z. Yang and S. Pan, Intriguing Structural Transition Inducing Variable Birefringences in ABa_2MS_4Cl (A = Rb, Cs; M = Ge, Sn), *Inorg. Chem.*, 2018, **57**, 11310–11313.

30 X. Ji, H. Wu, B. Zhang, H. Yu, Z. Hu, J. Wang and Y. Wu, Intriguing Dimensional Transition Inducing Variable Birefringence in $K_2Na_2Sn_3S_8$ and $Rb_3NaSn_3Se_8$, *Inorg. Chem.*, 2021, **60**, 1055–1061.

31 T. Tian, Z. Li, N. Wang, S. Zhao, J. Xu, Z. Lin and D. Mei, $Cs_2ZnSn_3S_8$: A Sulfide Compound Realizes a Large Birefringence by Modulating the Dimensional Structure, *Inorg. Chem.*, 2021, **60**, 9248–9253.

32 P. E. Blochl, Projector augmented-wave method, *Phys. Rev. B: Condens. Matter*, 1994, **50**, 17953–17979.